NUSC Technical Report 4583

# Modeling of Line-Array Transducers Near Finite-Width Soft Reflectors

RONALD P. RADLINSKI
*Sonar Technology Department*


10 July 1973

NAVAL UNDERWATER SYSTEMS CENTER
*New London Laboratory*

## ADMINISTRATIVE INFORMATION

This report was prepared under NUSC Project No. A-716-00, "Transducer Mathematical Modeling," Principal Investigator, Dr. C. H. Sherman (Code TD121), and Navy Subproject and Task No. SF 11 121 302-14077, Program Manager, R. Kolesar (NAVSHIPS PMS-302-421).

The author wishes to express his appreciation to Dr. Sherman, the Technical Reviewer, who encouraged this study and made numerous helpful suggestions, and Dr. P. H. Rogers, who made available the NRL data for the line source with a parabolic reflector.

REVIEWED AND APPROVED: 10 July 1973

W. A. Von Winkle
Director of Science and Technology

Inquiries concerning this report may be addressed to the author,
New London Laboratory, Naval Underwater Systems Center,
New London, Connecticut 06320

NAVAL POSTGRADUATE School

NAVAL UNDERWATER SYSTEMS CENTER
HEADQUARTERS
NEWPORT, RHODE ISLAND 02840

NEWPORT, R. I. 02840
AREA CODE 401
841 – EXT.
AUTOVON 948 + EXT.

NEW LONDON, CONN. 06320
AREA CODE 203
442 – 0771 – EXT.
AUTOVON 636 + EXT.

IN REPLY REFER TO:
LA152:SK:bw
5600
Ser: LA152-323

8 AUG 1973

From: Commanding Officer, Naval Underwater Systems Center
To: Distribution List

Subj: Forwarding of document

Encl: (1) NUSC Technical Report 4583, "Modeling of Line-Array Transducers Near Finite-Width Soft Reflectors," (U), dated 10 July 1973

1. Enclosure (1) is forwarded for information and retention.

S. KALKUS
By direction

Distribution List
Naval Ship Systems Command Headquarters, SHIPS 03, cy 2
SHIPS 031, cy 3
SHIPS 035, cy 4
SHIPS 2052, cy 5, 6, 7, 8
PMS-302, cy 9
PMS-302-4, cy 10
PMS-302-43, cy 11
PMS-302-5, cy 12
PMS-302-421, cy 13
Deputy Director for Defense Research & Engineering (S. Peterson), cy 14, 15
Chief of Naval Research, Code 468, cy 16
Chief of Naval Operations, OP-981H, cy 17
Chief of Naval Material, MAT-03, cy 18
Naval Undersea Center, Pasadena Lab., cy 19
Naval Ship Research & Development Center, Annapolis, cy 20
Naval Ship Research & Development Center, Carderock, cy 21
Naval Research Lab., (A. L. Von Buren, P. Rogers), cy 22, 23, 24
Naval Research Lab., Underwater Sound Reference Division, cy 25
Naval Oceanographic Office, Code 7200, cy 26
Code 9320, cy 27
Naval Ordnance Systems Command Headquarters, ORD-0632, cy 28
ASW Systems Project Office, ASW-22, cy 29
Naval Ship Research & Development Laboratory, Bethesda, cy 30
Naval Ordnance Laboratory, White Oak, cy 31
Naval Undersea Center, San Diego, cy 32

LA152:SK:bw
5600
Ser: 323

Distribution List - Con't

Naval Postgraduate School, Monterey, cy 33
Applied Physics Laboratory, University of Washington, Seattle, cy 34
Applied Research Laboratory, Pennsylvania State University, cy 35
Defense Documentation Center, cy 36-47
Marine Physical Laboratory, Scripps Institution of Oceanography, cy 48
National Research Council (Commander Undersea Warfare), cy 49
Woods Hole Oceanographic Institution, cy 50
John Butler, Raytheon Corp., Portsmouth, R. I., cy 51
M. Simon, Electric Boat Division of General Dynamics Corp., Groton, (Mechnical Engineering Branch), cy 52

UNCLASSIFIED
Security Classification

DOCUMENT CONTROL DATA - R & D

(Security classification of title, body of abstract and indexing annotation must be entered when the overall report is classified)

1. ORIGINATING ACTIVITY (Corporate author)
Naval Underwater Systems Center
Newport, Rhode Island 02840

2a. REPORT SECURITY CLASSIFICATION
UNCLASSIFIED

2b. GROUP

3. REPORT TITLE
MODELING OF LINE-ARRAY TRANSDUCERS NEAR FINITE-WIDTH SOFT REFLECTORS

4. DESCRIPTIVE NOTES (Type of report and inclusive dates)
Research Report

5. AUTHOR(S) (First name, middle initial, last name)
Ronald P. Radlinski

6. REPORT DATE
10 July 1973

7a. TOTAL NO. OF PAGES
36

7b. NO. OF REFS
9

8a. CONTRACT OR GRANT NO.

b. PROJECT NO. A-716-00
SF 11 121 302-14077

c.

d.

9a. ORIGINATOR'S REPORT NUMBER(S)
TR 4583

9b. OTHER REPORT NO(S) (Any other numbers that may be assigned this report)

10. DISTRIBUTION STATEMENT
Approved for public release; distribution unlimited.

11. SUPPLEMENTARY NOTES

12. SPONSORING MILITARY ACTIVITY
Department of the Navy

13. ABSTRACT

Farfield directivity patterns for line-array transducers with finite-aperture pressure-release reflectors are calculated by using a two-dimensional source-strength integral method. The directivity patterns obtained with plane and wedge reflectors are shown for both single and multiple sources. Normalized radiation impedances are calculated in order to determine the source-reflector and the source-source interactions. The effects of source size and reflector width are also investigated.

The accuracy of the numerical technique is determined by comparing calculated predictions with the measured nearfield and farfield pressure distributions from a line source at the focus of a parabolic reflector. Methods of resolving apparent anomalies in the numerical integral solution are also discussed.

DD FORM 1 NOV 65 1473 (PAGE 1)
S/N 0102-014-6600

UNCLASSIFIED
Security Classification

| 14. KEY WORDS | LINK A | | LINK B | | LINK C | |
|---|---|---|---|---|---|---|
| | ROLE | WT | ROLE | WT | ROLE | WT |
| Finite-Aperture Soft Reflectors | | | | | | |
| Line Arrays | | | | | | |
| Two Dimensional Source Strength Integral Method | | | | | | |
| Mathematical Modeling | | | | | | |

## ABSTRACT

Farfield directivity patterns for line-array transducers with finite-aperture pressure-release reflectors are calculated by using a two-dimensional source-strength integral method. The directivity patterns obtained with plane and wedge reflectors are shown for both single and multiple sources. Normalized radiation impedances are calculated in order to determine the source-reflector and the source-source interactions. The effects of source size and reflector width are also investigated.

The accuracy of the numerical technique is determined by comparing calculated predictions with the measured nearfield and farfield pressure distributions from a line source at the focus of a parabolic reflector. Methods of resolving apparent anomalies in the numerical integral solution are also discussed.

TABLE OF CONTENTS

# LIST OF ILLUSTRATIONS

## LIST OF ILLUSTRATIONS (Cont'd)



## LIST OF TABLES

# MODELING OF LINE-ARRAY TRANSDUCERS NEAR FINITE-WIDTH SOFT REFLECTORS

## INTRODUCTION

This report describes the use of a two-dimensional source-strength integral method to predict the directivity patterns and radiation impedances of line-array transducers with finite-aperture soft reflectors. This two-dimensional approach utilizes the fact that the line arrays and the reflector are long in comparison with the acoustical wavelengths of interest.

The specific goal is to examine the feasibility of constructing one or more high-power sources, backed by compliant reflectors, designed to provide a broad forward-searching beam. Primary consideration will be given to the directionality provided by plane and wedge reflectors. Line arrays composed of piezoelectric ceramic rings, magnetostrictive rings, or bender bars are examples of possible sources; candidates for reflector materials include compliant tubes and rubber tiles filled with a pressure-release material. Representative reflectors and sources are shown in figure 1.

## SOURCE-STRENGTH INTEGRAL METHOD

### FOURIER SERIES APPROACH

Consider the acoustical radiation from the arbitrary two-dimensional surface S shown in figure 2. The pressure at a field point t is given by the closed integral

$$P_t = \int A(s', k)\, \phi(s', t)\, d\vec{l}\,,$$

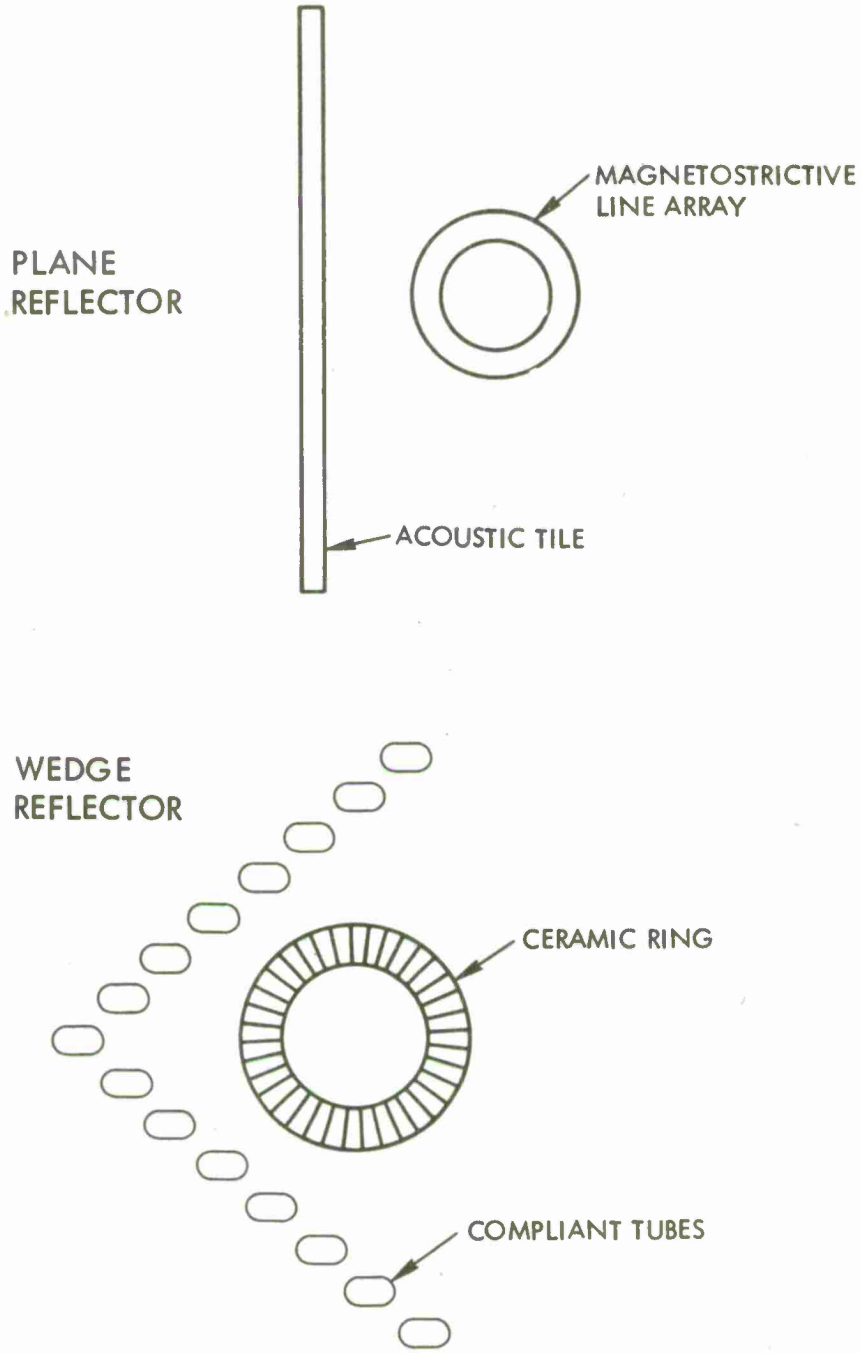


Figure 1. Representative Line Arrays and Reflectors

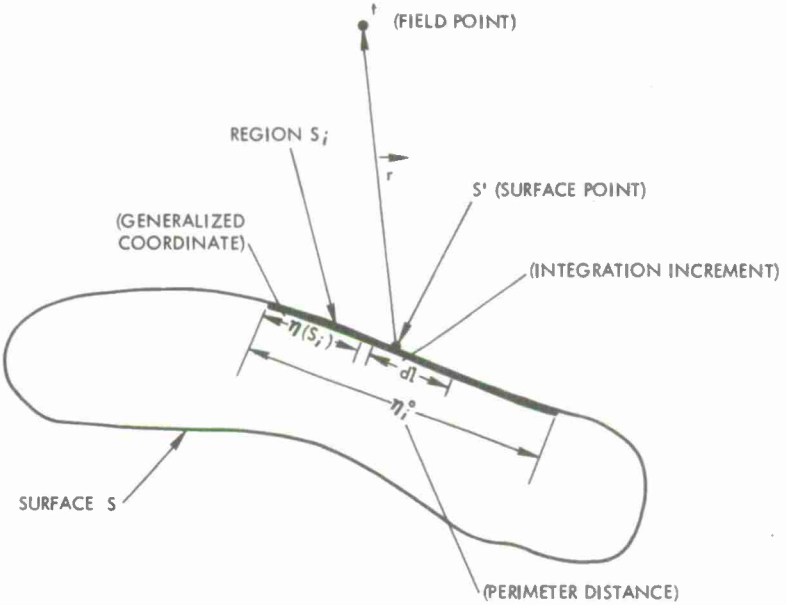


**Figure 2. Coordinates for the Numerical Integral Method**

where $\phi(s',t) = J_0(kr) + iY_0(kr)$ is the zeroth-order Hankel function of the first kind, k is the wave number, and $A(s',k)$ is the unknown source distribution on the surface. As shown by Liu and Martenson,[1] the source distribution for a given region $s_i$ on the surface S can be expressed in terms of a finite Fourier series as

$$A(s_i,k) = \sum_{m=1}^{M} \left\{ a_{m_i}(k) \sin\left[\frac{2\pi m\ \eta(s_i)}{\eta_i^o}\right] + b_{m_i}(k) \cos\left[\frac{2\pi(m-1)\ \eta(s_i)}{\eta_i^o}\right] \right\} ,$$

where $a_{m_i}(k)$ and $b_{m_i}(k)$ are the undetermined Fourier coefficients, and $\eta_i^o$ is the perimeter distance of the coordinate $\eta(s_i)$ on the i-th region (see figure 2).

The unknowns are the undetermined Fourier coefficients. For a surface of a given geometry, the regions are chosen so that the source distribution varies as smoothly as possible. At low frequencies, a few Fourier coefficients will often adequately describe the series. In this case, the number of unknowns (2M) can be taken to be less than the number of finite elements used for the numerical integrations. Therefore, there are fewer matrix elements than with

conventional approaches. As the frequency increases, there is no advantage in the Fourier method because the maximum number of terms is necessary to obtain series convergence.

The unknown coefficients are found by satisfying boundary conditions that may be specified in terms of normal velocity, pressure, or mechanical impedance. Matrix manipulations are accomplished by using the method of least squares. More complete details of the numerical technique are found in reference 2.

## NUMERICAL PITFALLS

When using a numerical integral method, one must be aware of the limitations of such an analysis. With the source-strength formulation, a solution involving a body at a Dirichlet eigenfrequency can be obtained only in a few particular cases, such as when the boundary conditions are specified in terms of zero pressure.[3] However, by using an interior surface, solutions were calculated at or near Dirichlet eigenfrequencies of bodies with nonzero impedance or velocity boundary conditions. As shown by Porter and Rogers,[4] the three-dimensional problem of active transducer bands on a finite solid cylinder can be recast into the case of bands on an annular cylinder, thereby eliminating the lower eigenfrequencies of the original solid body. In two dimensions, the introduction of an inner surface not only raises the frequency of the first eigenvalue, but it does not affect the exterior solution to the original problem. For instance, the eigenfrequencies of infinite cylinders occur at the zeros of the zeroth-order Bessel function or at $J_0(ka) = 0$, where $k$ is the wave number and $a$ is the radius of the cylinder. If the solid infinite cylinder is replaced by an infinite annular cylinder, the first Dirichlet eigenvalue occurs at a much higher frequency, as can be shown by solving the interior problem of the annulus with pressure-release boundary conditions.[5] Inasmuch as the inside of the annular surface is infinitely long, it should have no effect on the exterior solution. The eigenvalue problem for a cylindrical source was found to be unaffected by the presence of a pressure-release reflector.

The wave numbers corresponding to the Dirichlet eigenfrequencies of a plane reflector of width $a$ and thickness $t$ are given by

$$k_{mn} = \pi\left[\left(\frac{m}{a}\right)^2 + \left(\frac{n}{t}\right)^2\right]^{1/2},$$

where m and n are integers. Eigenvalue effects occurring for nonzero-pressure boundary conditions can be avoided either by choosing the reflector to be a fraction of a wavelength in thickness or by using an interior surface. However, one must also be careful not to model a reflector whose boundary conditions are specified in terms of velocity or nonzero impedance with a thickness less than about $\lambda/10$.* As shown in figure 3,† the numerical solution for a plate of thickness $\lambda/10 (kt=\pi/5)$ with a vibrating element of $k\Delta = 1.0$ on a rigid baffle with a dimensionless width of $kd = 13.6$ compares favorably with a series solution by Douglass[6] for a similar plate of negligible thickness. The numerical solution resulting from decreasing the plate thickness to $\lambda/20$ is shown, in figure 4, to be in poor agreement with the series solution for the radiation into the backward hemisphere. The comparisons continue to deteriorate when modeling plates thinner than those discussed above. For problems involving soft reflectors whose boundary conditions were satisfied in terms of pressure, the thinness of the reflector was not found to be critical to a solution. In all the following numerical examples, the reflectors were chosen to be $\lambda/10$ thick.

## COMPARISON OF NUMERICAL SOLUTIONS WITH NRL PARABOLIC-REFLECTOR DATA

To check the validity of the two-dimensional model, and also the accuracy of the numerical method, comparisons were made with reflector data from controlled experiments[7] performed at the Naval Research Laboratory (NRL). The data include radiation patterns obtained by using a USRD type F36 hydrophone[8] as the source and a pressure-release parabolic reflector. The hydrophone was 8 in. high and had an active diameter of 0.75 in. The reflector was 16 in. high and had a focal length of 4.0 in. and an aperture width of 28.4 in.; the surface of the reflector consisted of neoprene closed-cell rubber bonded to a copper sheet and was supported in a wooden frame. The frequencies considered in this experiment were such as to ensure that little radiation would be scattered into the backward hemisphere; hence, the specific modeling of the back of the reflector is unimportant.

*This limitation on the numerical technique was presented by Dr. Murray Simon, Electric Boat Division, General Dynamics Corporation.

†Figures 3 through 18 appear together, following the text, beginning on page 12.

Comparisons between the experimental measurements and the median-plane patterns predicted by means of the numerical method are shown in figures 5 through 8. The curves show nearfield and farfield data at the ends of the experimental frequency range. At 10 kHz, 7.5 finite-elements per wavelength were used in modeling the reflector. For both the nearfield and farfield (figures 5 and 6), the computations follow the experimental data within 2 dB. Since the computation time increases by at least the square of the number of elements, at 40 kHz the reflector was modeled with 4.25 elements per wavelength to keep the total computer execution time* less than 20 minutes. As seen in figure 7, the experimental measurements at 40 kHz are closely predicted in the nearfield. However, in the farfield, figure 8, the measured side lobes are suppressed as much as 6 dB in comparison with the numerical predictions. It is expected that if the number of elements per wavelength were increased to 7.5 at 40 kHz, the model discrepancies would be decreased.

Other sources of error arise from the use of straight-line elements to model curved surfaces and the assumption that the rubber-air composite is 100 percent reflective. In the frequency range of concern in the next two sections, a computational time limit of 10 minutes allows the use of at least 7.5 elements per wavelength. Also, since the plane and wedge reflectors are modeled with line-segment finite elements, curvature errors will arise only from the modeling of the cylindrical sources.

## MODELING OF A SINGLE SOURCE WITH A PLANE OR WEDGE REFLECTOR

To minimize the complexity of reflector construction, plane and wedge-shaped reflectors were investigated as a means of providing directionality for high-intensity sources. For long-range systems, where the time for ping return is substantial, broad transmit beams provide a means of minimizing the scan time. A minimum beamwidth of 90°, the width of the main lobe at the 3-dB downpoint, is desirable in this sense. In all the following examples, the sources are assumed to be vibrating uniformly with a unit velocity.

The method of images can be used as a guide to the expected forward-hemisphere patterns for a given placement of the source. The problem of a source near infinite-width wedge reflectors with opening angles of 180/n,

*On the EXEC II system of the Univac 1100 computer.

$n = 1, 2, 3, \ldots$ is amenable to solution by a finite number of image sources. This is valid for either line sources or sources of finite radius. As an example, the solution to a line source placed at $\lambda/4$ distance from a soft infinite plane is obtained by replacing the plane with an image source of opposite sign located at $-\lambda/4$. In figure 9, the image solution is compared in the farfield with that of the numerical integral solution for a $\lambda/50$-radius source placed at $\lambda/4$ distance from a $5\lambda$-wide pressure-release plane. As shown by the dashed curve, the image technique gives a solution only in the forward hemisphere. The integral solution, shown by the solid curve, illustrates the effects of the finite baffle by the radiation found in the backward hemisphere.

Next consider the effects of a finite-width soft reflector on a $\lambda/5$-radius cylinder vibrating with uniform velocity. In figure 10, the normalized farfield pattern when this cylinder is placed at $\lambda/4$ distance from the center of a $5\lambda$ plane reflector is compared with the pattern for a $\lambda/50$-radius source placed at the same location. The larger source has a higher directivity, but to a first approximation the patterns are almost independent of the source size. With the $\lambda/5$-radius source, the beamwidth is about 100°, and the normalized pressure is down 18 dB at 90°. The normalized radiation impedance per unit length was determined by integrating the pressure over the circumference of the cylinder and dividing by the product of the circumference times the $\rho c$ of water. For the $\lambda/5$-radius cylinder in front of the $5\lambda$ reflector, the calculated radiation resistance shown in table 1 is about 76 percent the value for the same size

Table 1. Normalized Radiation Impedance per Unit Length for a Single Source with Reflector

| Reflector | Aperture | Source Radius | Horizontal Distance of Source Center from Midpoint of Reflecting Surface | Radiation Resistance* (per unit length) | Radiation Reactance* (per unit length) |
|---|---|---|---|---|---|
| Plane | $5\lambda$ | $\lambda/5$ | $\lambda/4$ | $0.649 \pm 0.005$ | $-0.482 \pm 0.006$ |
| Plane | $3\lambda$ | $\lambda/5$ | $\lambda/4$ | $0.658 \pm 0.004$ | $-0.482 \pm 0.005$ |
| Plane | $1\lambda$ | $\lambda/5$ | $\lambda/4$ | $0.666 \pm 0.003$ | $-0.484 \pm 0.004$ |
| 120° Wedge | $5\sqrt{3}\lambda/2$ | $\lambda/3$ | $\lambda/2$ | $0.713 \pm 0.023$ | $-0.498 \pm 0.025$ |
| 90° Wedge | $5\lambda/\sqrt{2}$ | $\lambda/3$ | $0.55\lambda$ | $0.542 \pm 0.018$ | $-0.473 \pm 0.024$ |

*The error bars are estimates of error introduced in the numerical integration.

cylinder uniformly vibrating without the reflector. Thus, for a given velocity distribution on the transducer, the desired directivity is gained at the cost of a 1/4 decrease in power radiated from the source.

For practical considerations, one would make the reflector as narrow as possible. Consider the effects of reducing the original $5\lambda$-wide reflector by increments of $2\lambda$. As seen in figure 11, placing the $\lambda/5$-radius source at $\lambda/4$ distance from the center of a $3\lambda$ reflecting surface results in a 90° beamwidth. In the plane of the reflector, a 2-dB increase in intensity results from the $2\lambda$ reduction in reflector width. For a $1\lambda$ reflector, shown in figure 12, the $\lambda/5$-radius source gives about an 80° beamwidth. The intensity at 90° is down by only 11 dB, and significant radiation is scattered into the backward hemisphere. In both of the above figures, the comparison of a $\lambda/50$-radius source with the $\lambda/5$-radius source again shows the small effect of source size on the farfield patterns. As the data in table 1 show, the radiation resistance of the $\lambda/5$-radius source increases by less than 3 percent as the reflector is reduced from $5\lambda$ to $1\lambda$.

To produce the desired broad beamwidths by using a soft plane reflector, the source has to be centered at $\lambda/4$ distance from the midpoint of the reflecting surface. This location restricts the size of the cylindrical source to less than $\lambda/4$ in radius. One method of increasing power output is to use a larger source with a wedge reflector. As an example, the calculated farfield pattern for a $\lambda/3$-radius source placed at $\lambda/2$ distance from the vertex of a 120° reflector is shown in figure 13. This wedge reflector has a $5\sqrt{3}\ \lambda/2$ aperture. Some sacrifice of beamwidth is evident from the 75° forward beam, and at 90° the intensity is down by almost 24 dB. The normalized radiation resistance per unit length given in table 1 for the $\lambda/3$-radius source is about 76 percent of the "free-field' radiation resistance of a $\lambda/3$-radius source in the absence of the reflector. The pattern for the $\lambda/50$-radius source with the 120° wedge reflector (as shown by the dashed curve in figure 13) has a similar shape to that produced by the $\lambda/3$-radius source, but, in this case, the directivity is greater with the smaller source.

Although wedge reflectors with opening angles less than 120° would not be expected to give broad beamwidths, 90° wedge reflectors were investigated because the results could be compared with predictions calculated by the image method. The source was placed at $\lambda/2$ distance so that the fields of all images would be in phase at 0°. In figure 14, the image solution for a line source placed at $\lambda/2$ distance from the vertex of a 90° wedge with an infinite aperture is compared with the finite-element solution for a $\lambda/50$-radius source at $\lambda/2$ distance from the vertex of a 90° wedge with a $5\lambda/\sqrt{2}$ aperture. The advantage of the

numerical method is evident in that the image technique gives a solution only in the forward 90° sector.

The effect of source size on the patterns obtained with a 90° reflector is shown in figure 15, where a comparison is made between radiation from a $\lambda/3$-radius source and from a $\lambda/50$-radius source, both placed at $0.55\lambda$ distance from the vertex of the 90° wedge. The source distance was changed to $0.55\lambda$ because placing a $\lambda/3$-radius cylinder at $\lambda/2$ distance from the vertex is a tight squeeze. Notice the essential lack of side lobes with either source. With the $\lambda/3$-radius source, the radiation resistance, as given in table 1, is about 58 percent of that for the same size cylindrical source without a reflector. Not surprisingly, the power output of a single source is decreased significantly when a larger portion of its surface is in close proximity to the reflector.

## MODELING OF MULTIPLE SOURCES WITH A PLANE OR WEDGE REFLECTOR

As another method of increasing power output, consider the effects of using two or more cylindrical sources with a single reflector. Curves proportional to the normalized radiation resistance per unit length, which are given in reference 9, show that, depending on the separation distance, the radiation resistance of each source can be increased or decreased with respect to that of a single source. It will be shown that by judicious placement of the sources one can both obtain the desired patterns and counteract undesirable source-reflector effects by utilizing the effects of interaction of the sources. Again, the method of images can be used in determining the placement of sources.

The first example of using multiple sources with a reflector is for two $\lambda/3$-radius sources vibrating with unit velocity and placed at $0.55\lambda$ and $1.25\lambda$ distances from the vertex of a 90° wedge reflector with an aperture of $5\lambda/\sqrt{2}$. The resulting pattern, as shown in figure 16, is a candidate for narrowbeam applications. The radiation resistance, given in table 2, for source 2 at $1.25\lambda$ distance differs by only 4 percent from that for source 1 at $0.55\lambda$ distance. The radiation resistance of source 1 is about 2.05 times the value given in table 1 for a single $\lambda/3$-radius source placed at $0.55\lambda$ distance from the 90° wedge reflector.

Now consider multiple sources near a finite plane reflector. The farfield pattern for two $\lambda/5$-radius sources with a center-to-center separation of $\lambda/2$, both placed at $\lambda/4$ distance from a $5\lambda$-wide pressure-release plane, is shown in figure 17. Although the beamwidth is only about 40°, the low directivity of the

Table 2. Normalized Radiation Impedance per Unit Length for Multiple Sources with a Reflector

| Reflector | Aperture | Source Number | Source Radius | Horizontal Distance of Source Center from Midpoint of Reflecting Surface | Vertical Distance of Source Center from Midpoint of Reflecting Surface | Radiation Resistance* (per unit length) | Radiation Reactance* (per unit length) |
|---|---|---|---|---|---|---|---|
| 90° Wedge | $5\lambda/\sqrt{2}$ | 1 | $\lambda/3$ | $0.55\lambda$ | — | $1.11 \pm 0.025$ | $+0.198 \pm 0.009$ |
| | | 2 | $\lambda/3$ | $1.25\lambda$ | — | $1.07 \pm 0.025$ | $-0.199 \pm 0.009$ |
| Plane | $5\lambda$ | 1 | $\lambda/5$ | $\lambda/4$ | $+\lambda/4$ | $1.14 \pm 0.01$ | $-0.563 \pm 0.011$ |
| | | 2 | $\lambda/5$ | $\lambda/4$ | $-\lambda/4$ | $1.14 \pm 0.01$ | $-0.563 \pm 0.011$ |
| Plane | $5\lambda$ | 1 | $\lambda/5$ | $\lambda/4$ | $+3\lambda/4$ | $1.00 \pm 0.02$ | $-0.605 \pm 0.017$ |
| | | 2 | $\lambda/5$ | $\lambda/4$ | $+\lambda/4$ | $1.44 \pm 0.03$ | $-0.949 \pm 0.026$ |
| | | 3 | $\lambda/5$ | $\lambda/4$ | $-\lambda/4$ | $1.44 \pm 0.03$ | $-0.949 \pm 0.026$ |
| | | 4 | $\lambda/5$ | $\lambda/4$ | $-3\lambda/4$ | $1.00 \pm 0.02$ | $-0.605 \pm 0.017$ |

*The error bars are estimates of error introduced in the numerical integration.

pattern makes this configuration a possible candidate for long-range systems. The radiation resistance of each of the $\lambda/5$-radius cylinders, as recorded in table 2, is about 1.35 times that for a single $\lambda/5$-radius cylinder vibrating without the reflector. Notice that the dashed curve in figure 17 (for two $\lambda/50$-radius cylinders and a reflector) varies considerably at wide angles from the pattern for the larger cylinders at the same locations.

The final example, shown in figure 18, is the result of placing four $\lambda/5$-radius sources in a line (with $\lambda/2$ center-to-center spacing between cylinders) at $\lambda/4$ distance from a $5\lambda$-wide plane. The outside cylinders have radiation resistances that are 1.18 times the free-field value for a $\lambda/5$ cylinder, and the radiation resistances of the inner cylinders are 1.44 times that of the outer ones. The main lobe of the pattern in figure 18 is similar to the narrow beam expected from a 90° wedge reflector. This configuration could be considered as an alternative method for obtaining high power with a narrow beamwidth.

## CONCLUSIONS

A two-dimensional source-strength integral method has been used to predict radiation impedances and farfield patterns for line-array transducers placed near pressure-release reflectors. Calculations from the mathematical model compare favorably with experimental data from a line source at the focal line of a parabolic reflector. The agreement between theory and experiment supports the validity of the method, which was subsequently applied to predicting radiation patterns involving reflectors of other shapes.

For plane and wedge reflectors, the method of images is useful in determining the placement of sources for producing a desired pattern. For sources less than 1/4 wavelength in radius, the desired broad-beamwidth patterns can be obtained with plane reflectors; in order to limit the amount of radiation scattered into the backward hemisphere, the width of the plane reflector should not be reduced to less than 3 wavelengths. Placing a 1/3-wavelength-radius source at 1/2 wavelength from the vertex of a 120° wedge reflector permits increasing the power and still maintaining a broad beamwidth. For the examples of a single source with a reflector, the shape of the radiation patterns did not depend appreciably on the source size.

The directionality attained with a soft reflector is accompanied by a significant decrease in the radiation resistance of the source; therefore, the radiated power is reduced. The increased radiation resistances that result from the mutual interaction of properly spaced multiple sources can be utilized to offset the effect of the reflector. Therefore, in cases where the source size is restricted, the use of multiple sources provides an alternative method of increasing power output.

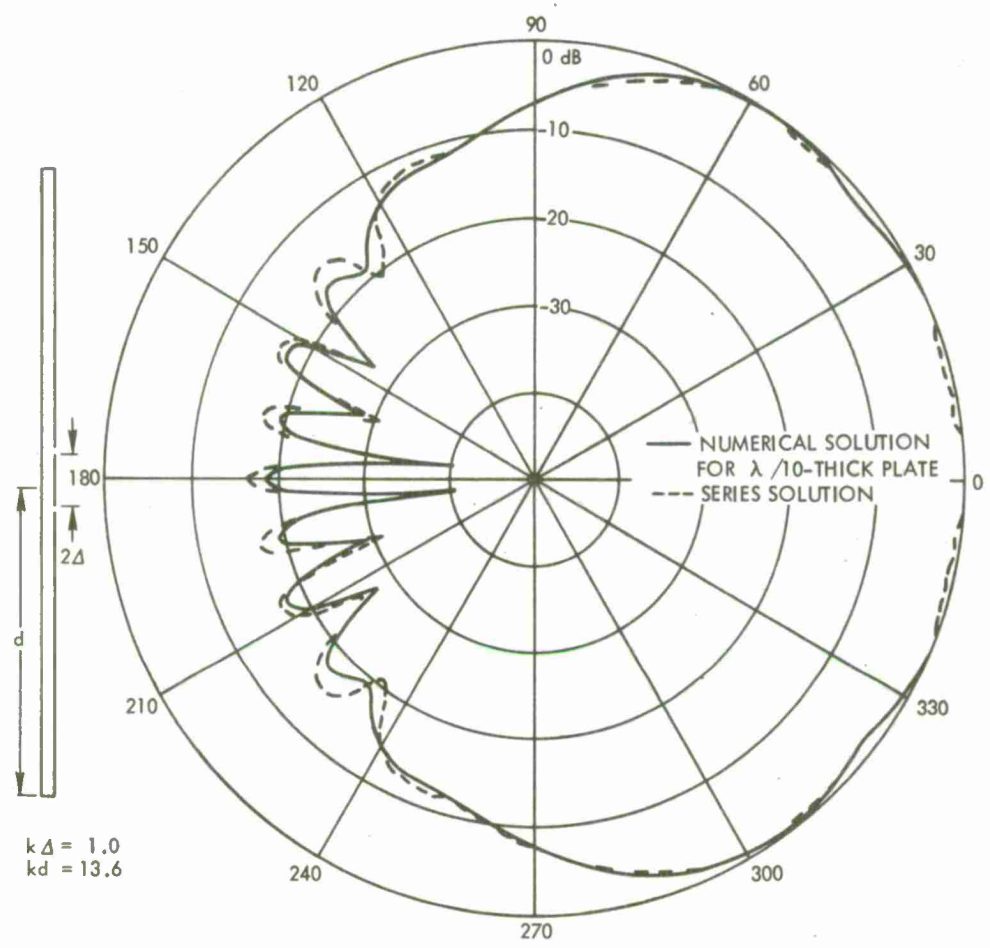


Figure 3. Comparison of an Elliptical Wave-Function Series Solution for a Plate of Negligible Thickness with the Numerical Integral Solution for a Plate λ/10 Thick

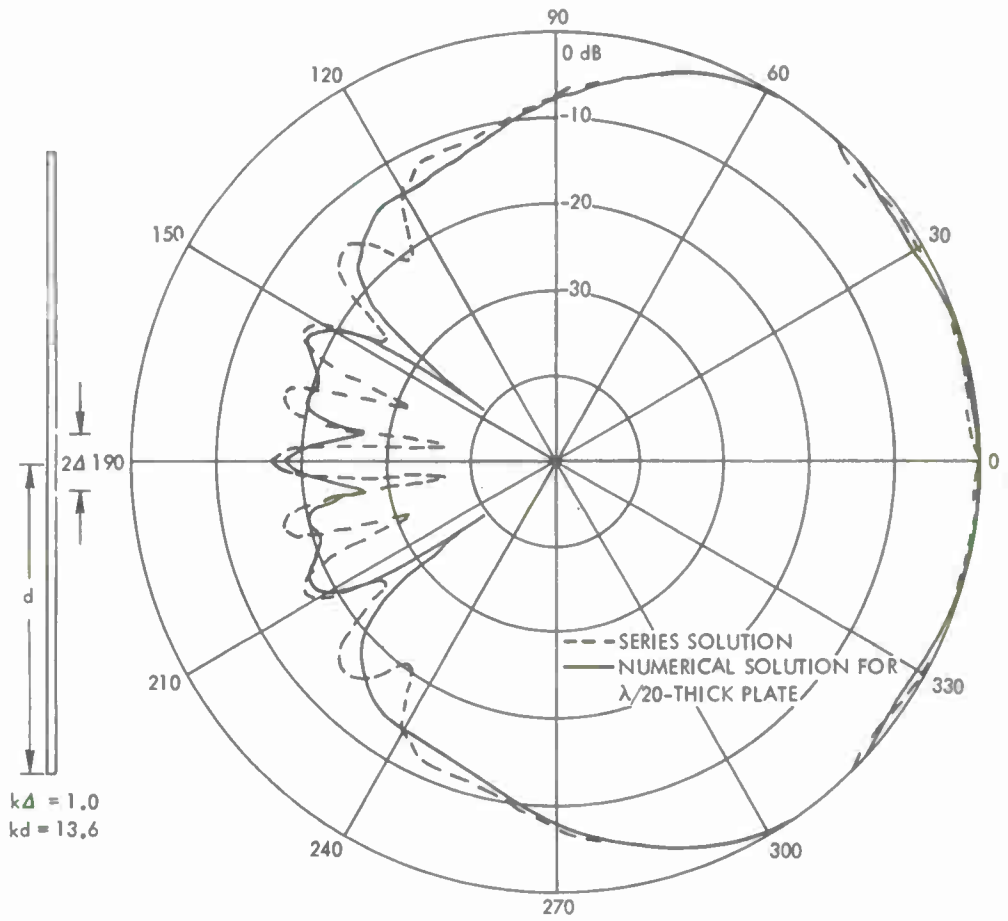


Figure 4. Comparison of an Elliptical Wave-Function Series Solution for a Plate of Negligible Thickness with the Numerical Integral Solution for a Plate λ/20 Thick

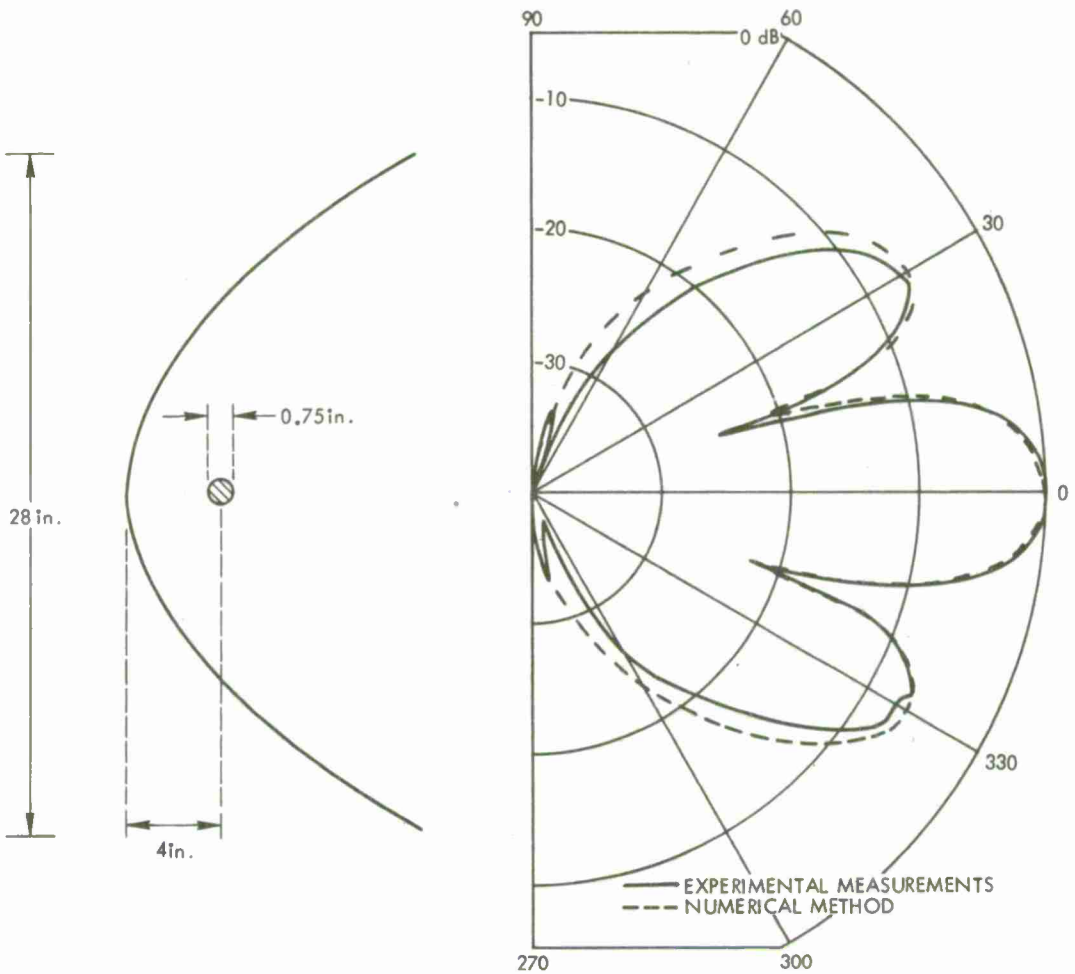


**Figure 5. Comparison of Nearfield 10-kHz Radiation Patterns for a Parabolic Reflector Obtained by Numerical Integral Method and from NRL Experimental Measurements**

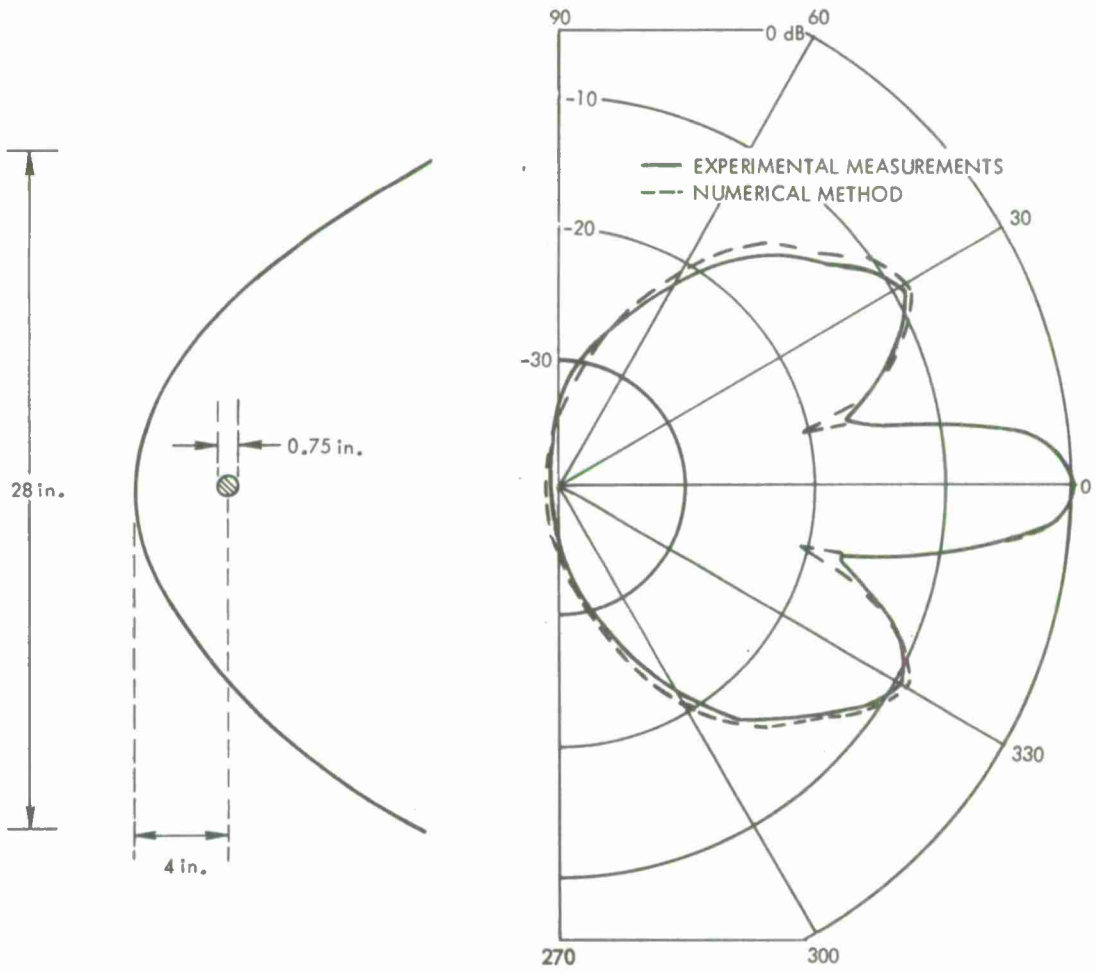


Figure 6. Comparison of Farfield 10-kHz Radiation Patterns for a Parabolic Reflector Obtained by Numerical Integral Method and from NRL Experimental Measurements

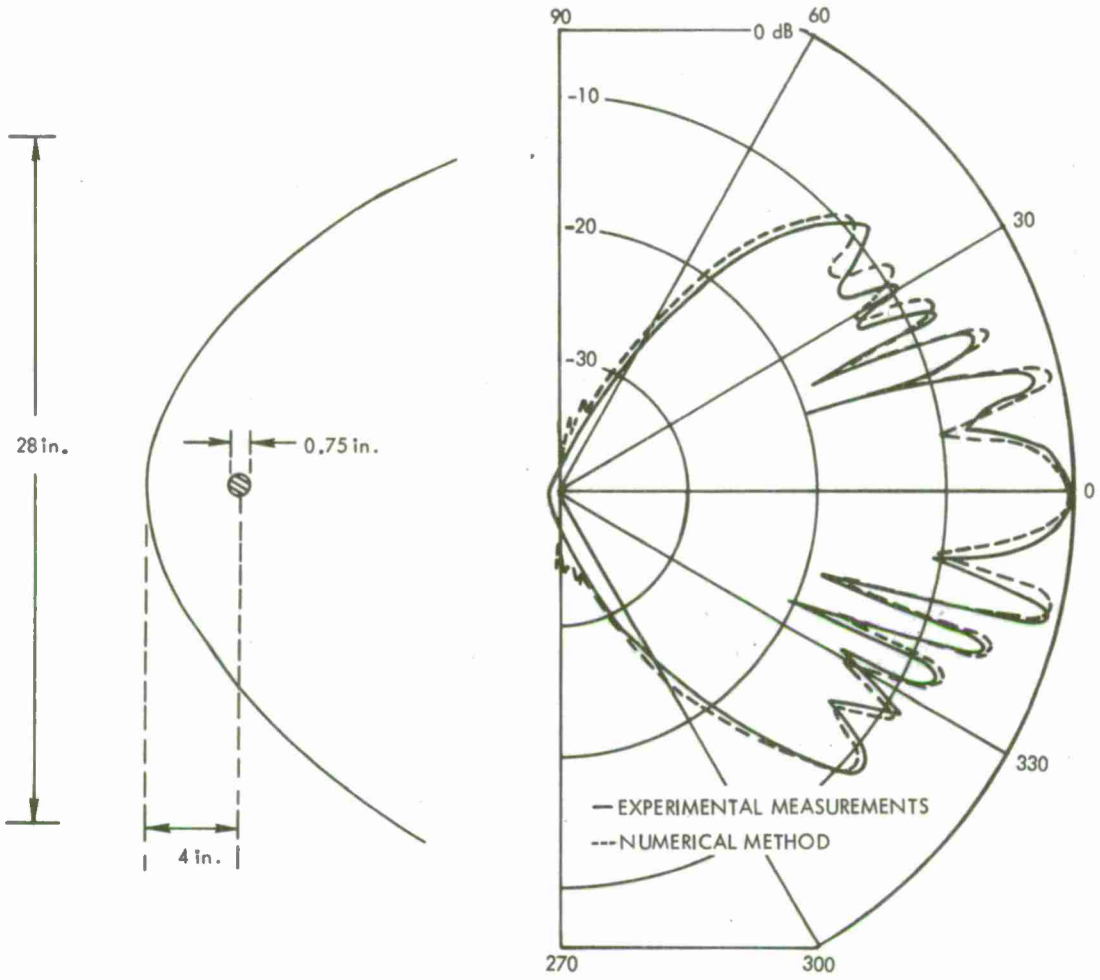


**Figure 7. Comparison of Nearfield 40-kHz Radiation Patterns for a Parabolic Reflector Obtained by Numerical Integral Method and from NRL Experimental Measurements**

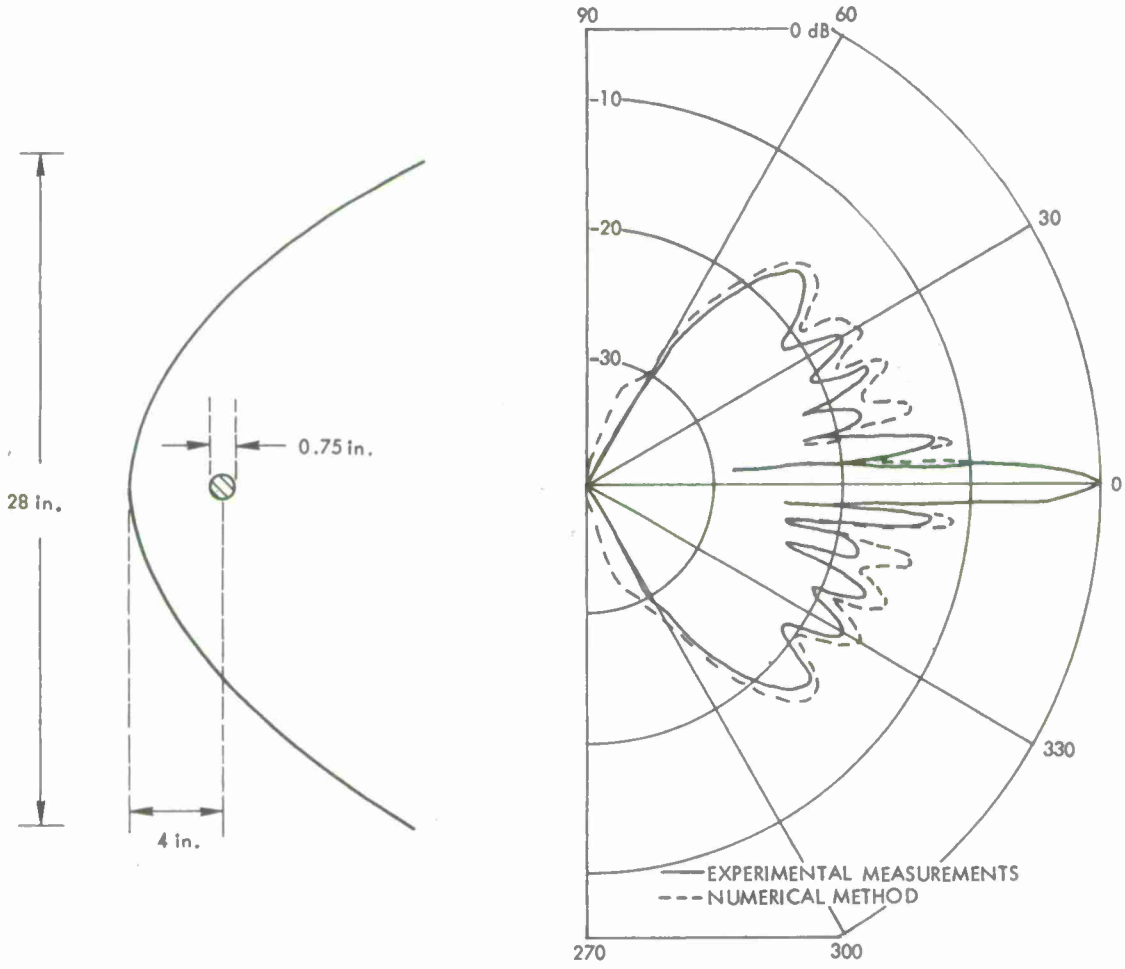


Figure 8. Comparison of Farfield 40-kHz Radiation Patterns for a Parabolic Reflector Obtained by Numerical Integral Method and from NRL Experimental Measurements

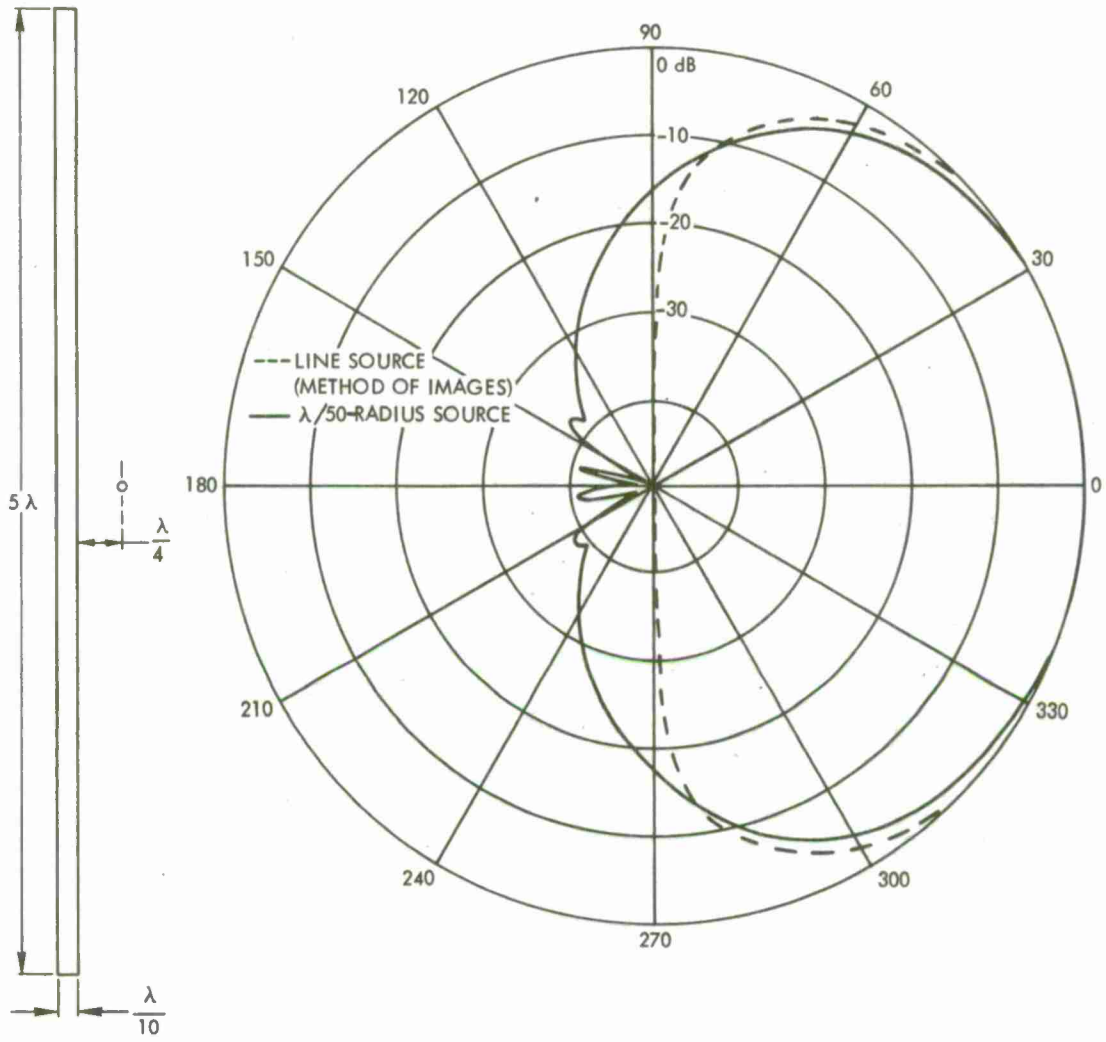


Figure 9. Comparison of Farfield Radiation Patterns for a λ/50-Radius Cylindrical Source at λ/4 Distance from a 5λ Pressure-Release Plane and for a Line Source at the Same Distance from an Infinite Plane

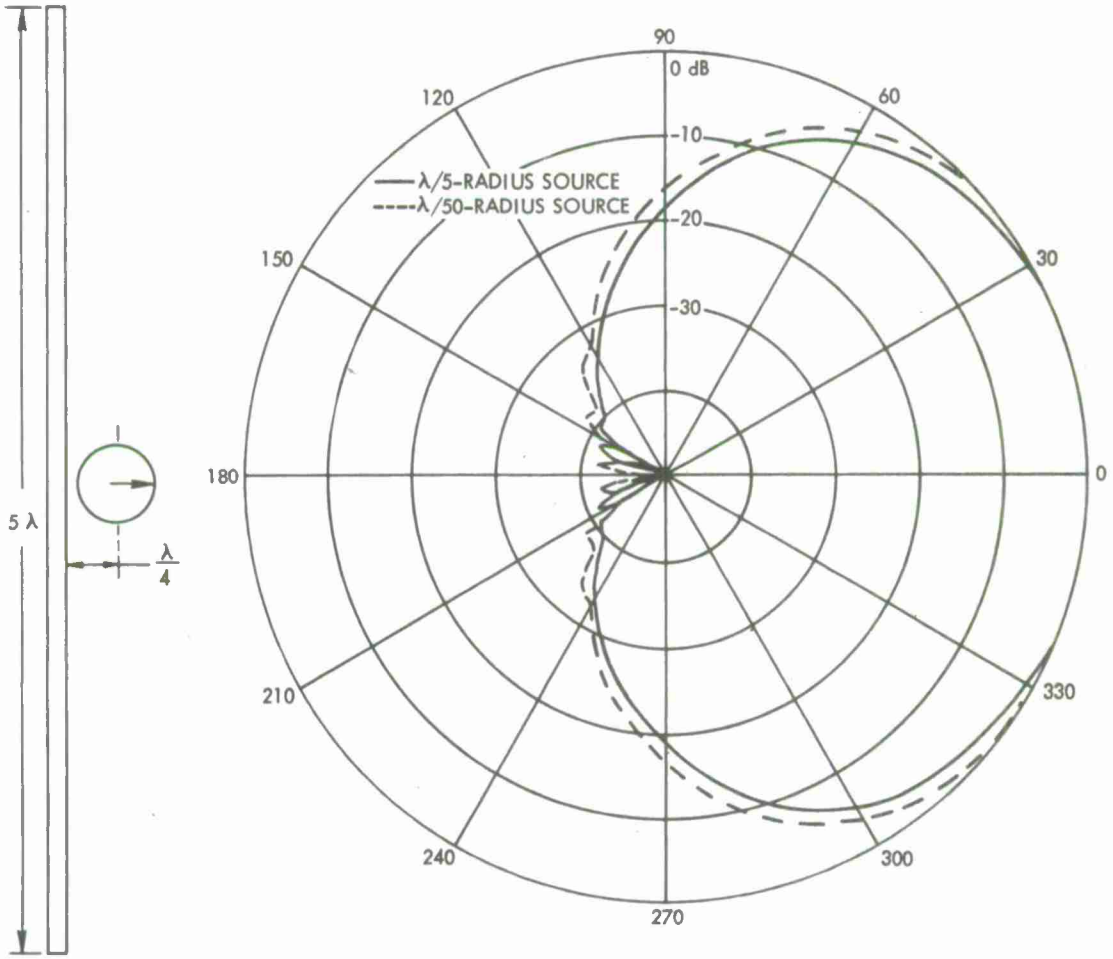


Figure 10. Comparison of Farfield Radiation Patterns for λ/5-Radius and λ/50-Radius Cylindrical Sources at λ/4 Distance from a 5λ Pressure-Release Plane

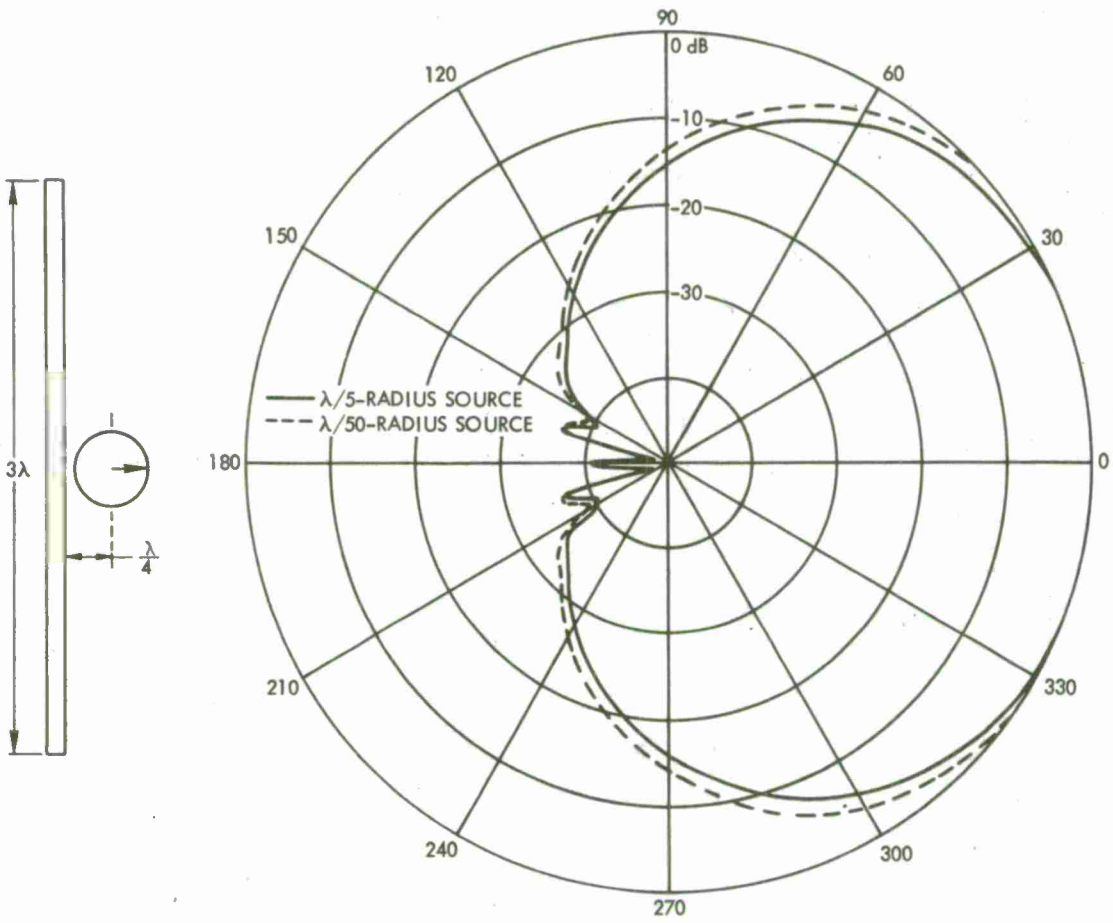


Figure 11. Comparison of Farfield Radiation Patterns for λ/5-Radius and λ/50-Radius Cylindrical Sources at λ/4 Distance from a 3λ Pressure-Release Plane

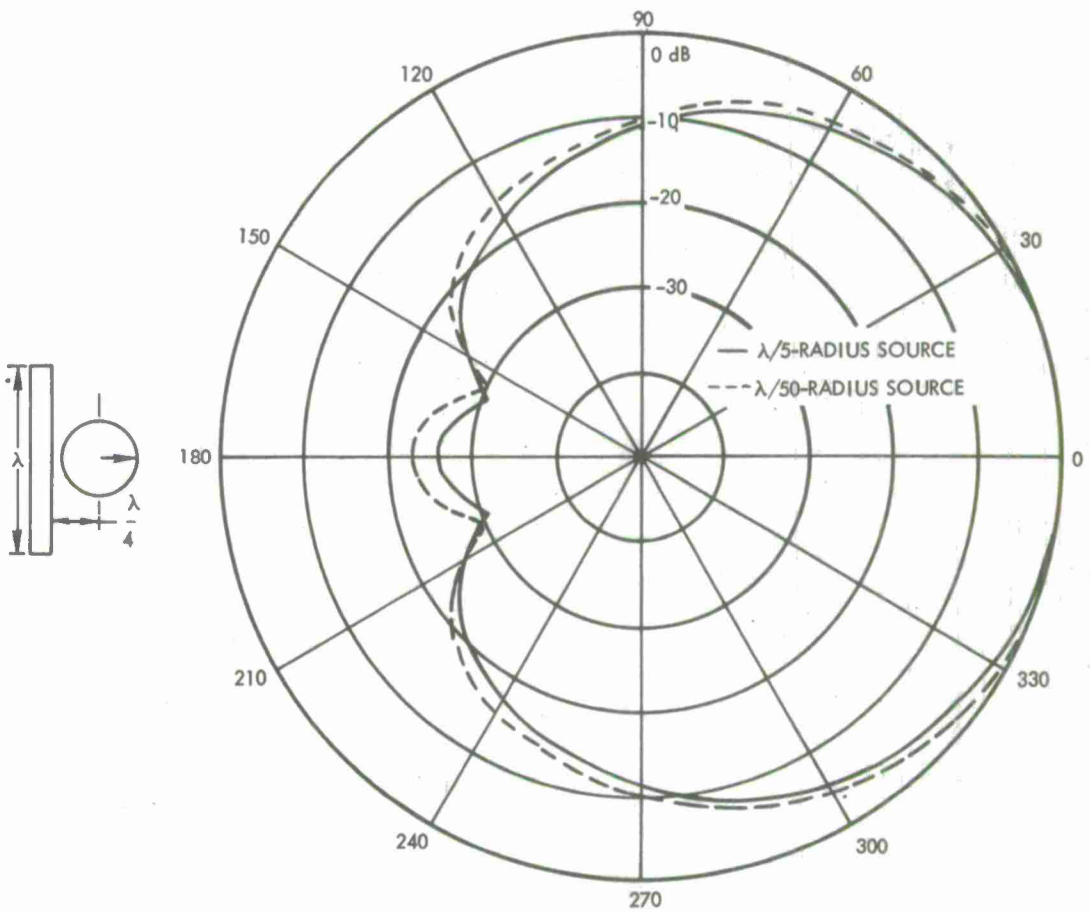


Figure 12. Comparison of Farfield Radiation Patterns for λ/5-Radius and λ/50-Radius Cylindrical Sources at λ/4 Distance from from a 1λ Pressure-Release Plane

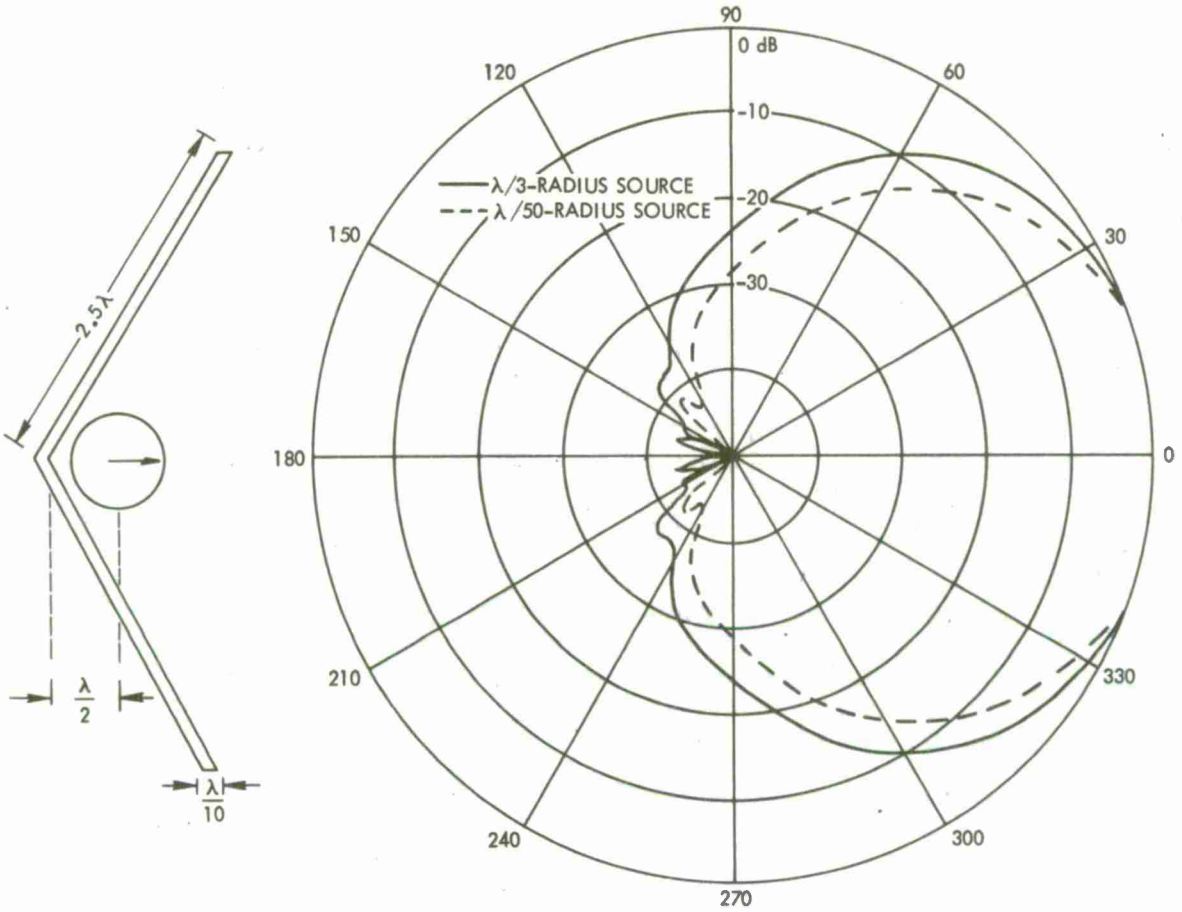


Figure 13. Comparison of Farfield Radiation Patterns for λ/3-Radius and λ/50-Radius Cylindrical Sources at λ/2 Distance from a 5λ 120° Pressure-Release Wedge

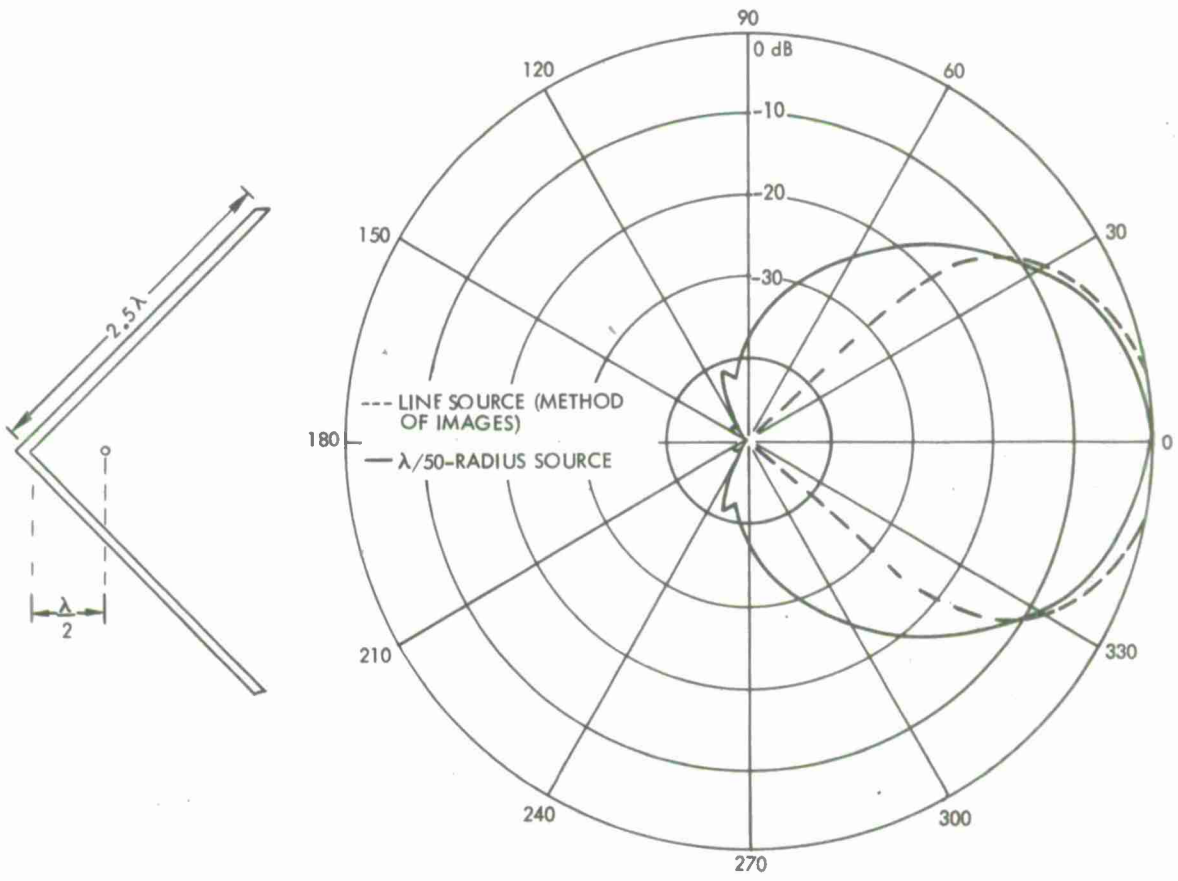


Figure 14. Comparison of Farfield Radiation Patterns for a λ/50-Radius Cylindrical Source at λ/2 Distance from a 5λ 90° Pressure-Release Wedge and for a Line Source at λ/4 Distance from an Infinite-Aperture 90° Pressure-Release Wedge

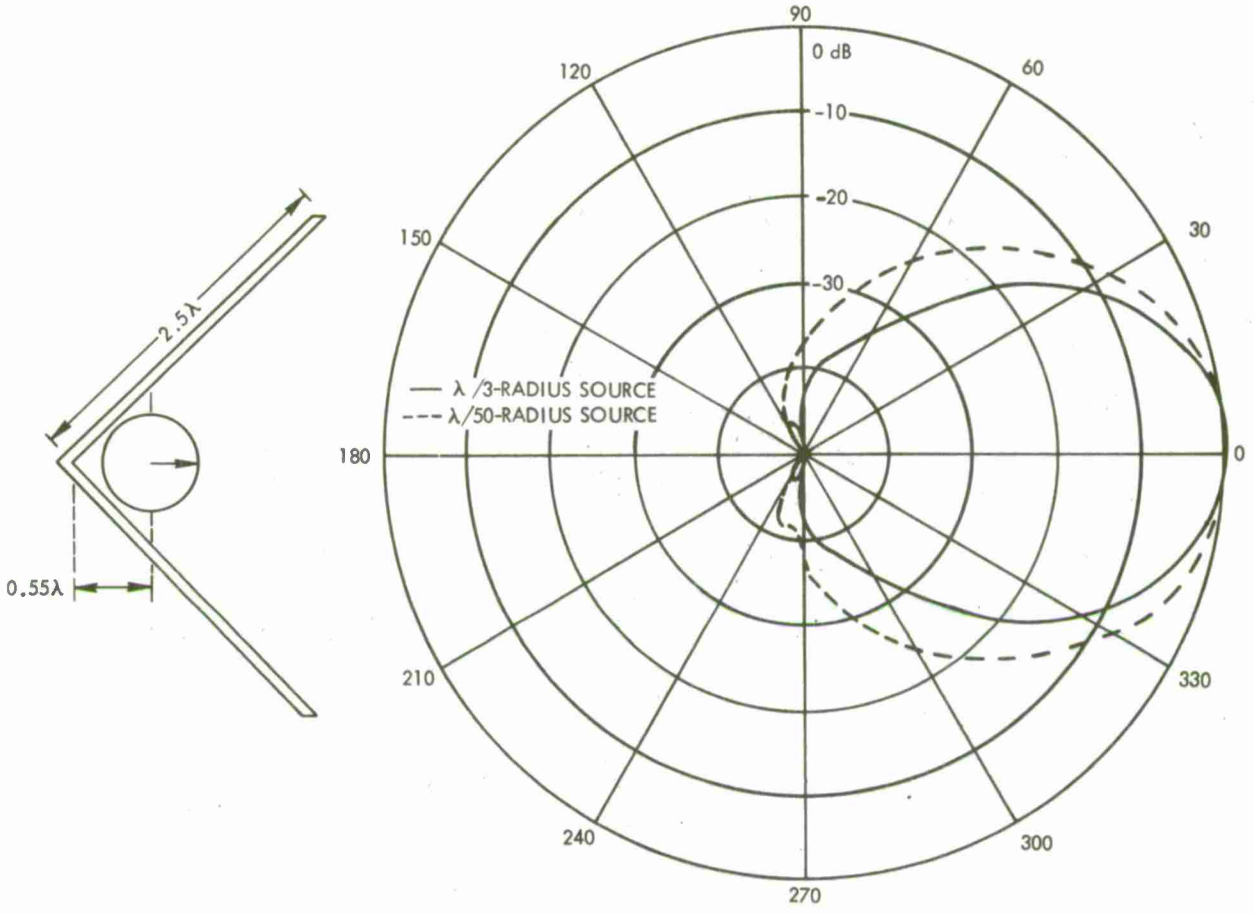


Figure 15. Comparison of Farfield Radiation Patterns for λ/3-Radius and λ/50-Radius Cylindrical Sources at 0.55λ Distance from a 5λ 90° Pressure-Release Wedge

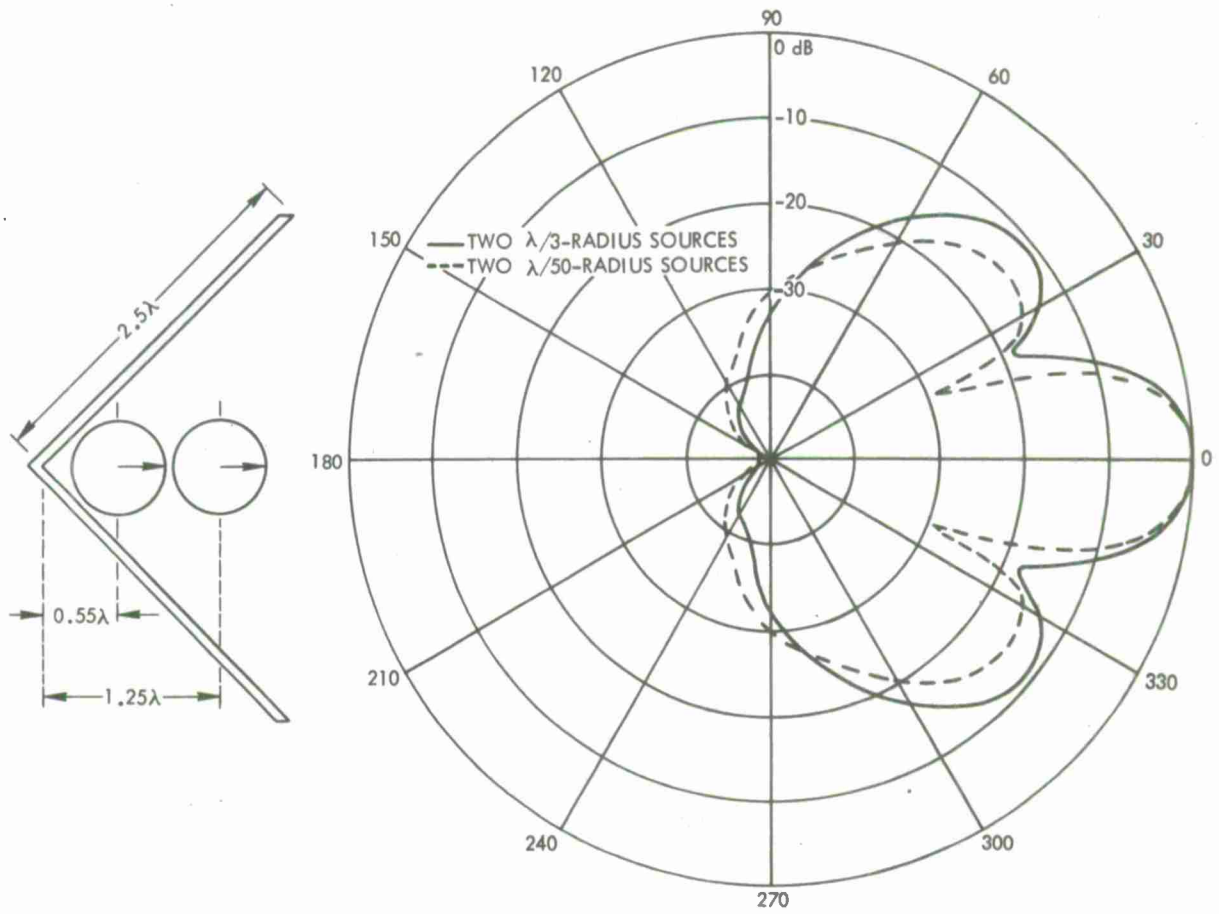


Figure 16. Comparison of Farfield Radiation Patterns for Two λ/3-Radius and Two λ/50-Radius Cylindrical Sources at 0.55λ and 1.25λ Distances from a 5λ 90° Pressure-Release Wedge

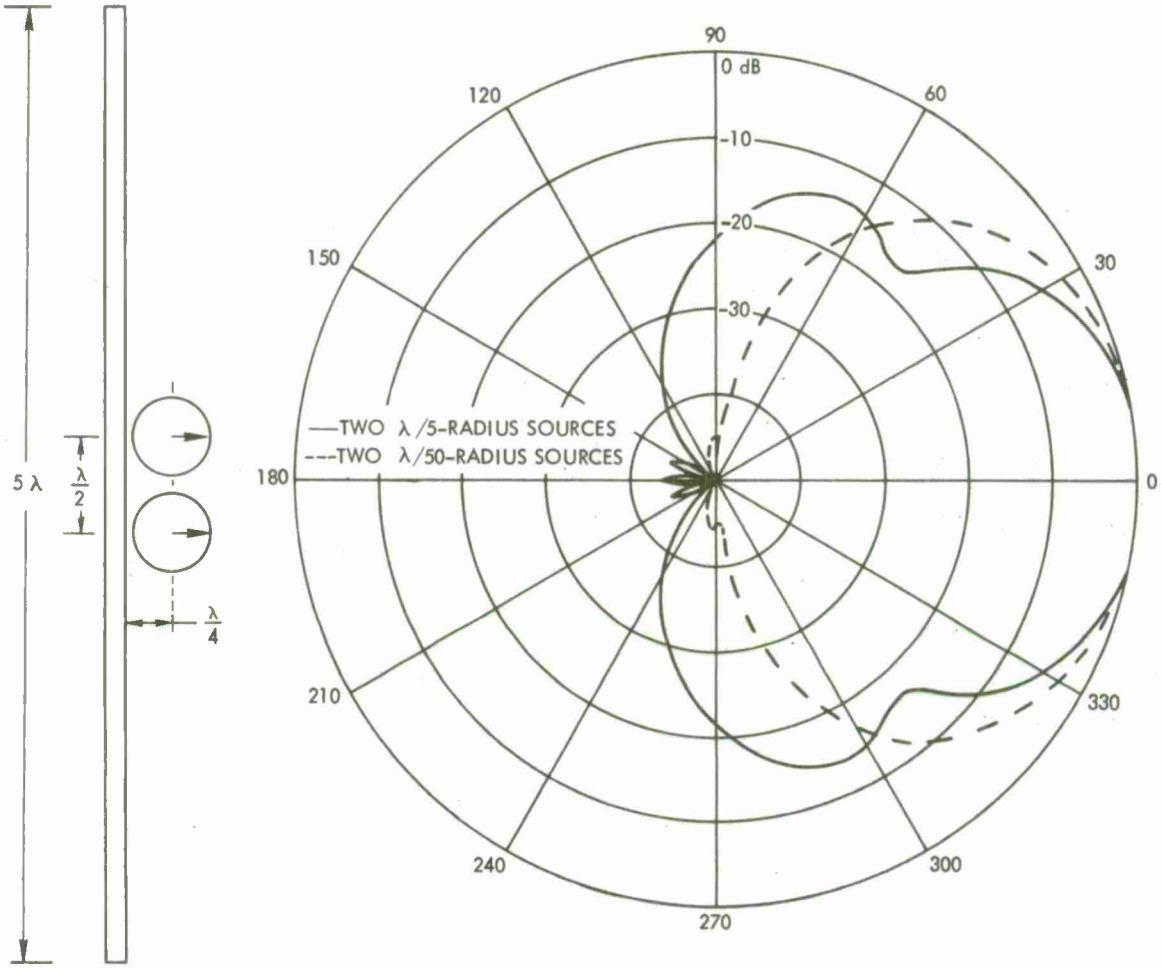


Figure 17. Comparison of Farfield Radiation Patterns for Two λ5/-Radius and Two λ/50-Radius Cylindrical Sources with λ/2 Separation at λ/4 Distance from a 5λ Pressure-Release Plane

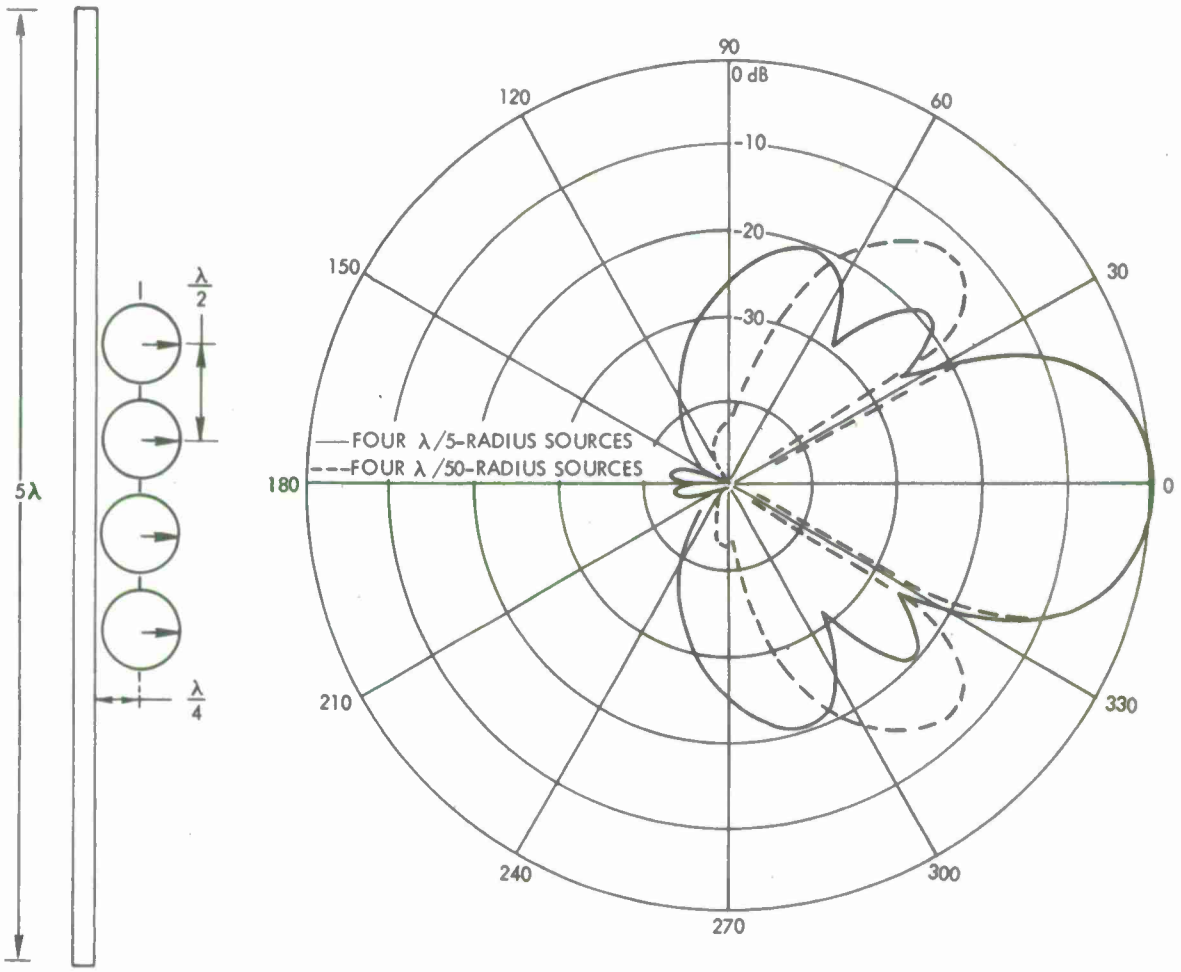


Figure 18. Comparison of Farfield Radiation Patterns for Four λ5/-Radius and Four λ/50-Radius Cylindrical Sources with λ/2 Separation at λ/4 Distance from a 5λ Pressure-Release Plane


REVERSE BLANK

## REFERENCES

1. H. K. Liu and A. J. Martenson, "A Numerical Technique for Solving Acoustic Radiation Problems," paper presented to the Acoustical Society of America meeting, Atlantic City, N. J., April 1970.

2. R. P. Radlinski, "A Computer Program for Solving Two Dimensional Radiation Problems by the Source Strength Integral Method," NUSC Technical Memorandum TD12-71-72, 25 February 1972.

3. G. Chertock, Integral Equation Methods in Sound Radiation and Scattering from Arbitrary Surfaces, NSRDC Report 3538, June 1971.

4. D. T. Porter and P. H. Rogers, "Radiation from an Array of Transducers on a Finite Cylinder," paper presented to the Acoustical Society of America meeting, Buffalo, N. Y., April 1972.

5. H. A. Schenck, "Improved Integral Formulation for Acoustic Radiation Problems," Journal of the Acoustical Society of America, vol. 44, no. 1, 1968, pp. 41-58.

6. R. E. Douglass," A Study of the Effects of Baffle Width on the Beam Patterns of Planar Arrays of Sonar Transducers," University of Texas dissertation, June 1967.

7. J. A. Sinsky, P. H. Rogers, and A. Bozzi, An Experimental Study of a Line Source Coincident with the Focal Line of a Parabolic Cylinder Reflector, NRL Report 7486, 20 December 1972.

8. R. J. Bobber, Underwater Electroacoustic Measurements, Naval Research Laboratory, Washington, D. C., 1970, pp. 251-252.

9. E. Skudrzyk, Simple and Complex Vibratory Systems, Pennsylvania State University Press, 1968, p. 368.

## INITIAL DISTRIBUTION LIST

Deputy Director for Defense Research & Engineering
Chief of Naval Research, Code 468
Chief of Naval Operations, Op-981H
Chief of Naval Material, MAT-03
Naval Undersea Center, Pasadena
Naval Ship Research & Development Center, Annapolis
Naval Ship Research & Development Center, Carderock
Naval Research Laboratory
Naval Research Laboratory, Underwater Sound Reference Division
Naval Oceanographic Office, Code 7200
Code 9320
Naval Ordnance Systems Command Headquarters, ORD-0632
Naval Ship Systems Command Headquarters, SHIPS-03
SHIPS-031
SHIPS-035
SHIPS-2052
PMS-302
PMS-302-4
PMS-302-43
PMS-302-5
PMS-302-421
ASW Systems Project Office, ASW-22
Naval Ship Research & Development Laboratory, Bethesda
Naval Ordnance Laboratory, White Oak
Naval Undersea Center, San Diego
Naval Postgraduate School, Monterey
Applied Physics Laboratory, University of Washington
Applied Research Laboratory, Pennsylvania State University
Defense Documentation Center (DDC)
Marine Physical Laboratory, Scripps Institution of Oceanography
National Research Council
Woods Hole Oceanographic Institution